

Accepted Manuscript

Title: A one-step method for preparation of Cu@Cu₂O nanoparticles on reduced graphene oxide and their catalytic activities in *N*-arylation of *N*-heterocycles

Author: Siyavash Kazemi Movahed Minoo Dabiri Ayoob Bazgir



PII: S0926-860X(14)00264-6
DOI: <http://dx.doi.org/doi:10.1016/j.apcata.2014.04.023>
Reference: APCATA 14796

To appear in: *Applied Catalysis A: General*

Received date: 21-9-2013
Revised date: 9-4-2014
Accepted date: 12-4-2014

Please cite this article as: S.K. Movahed, M. Dabiri, A. Bazgir, A one-step method for preparation of Cu@Cu₂O nanoparticles on reduced graphene oxide and their catalytic activities in *N*-arylation of *N*-heterocycles, *Applied Catalysis A, General* (2014), <http://dx.doi.org/10.1016/j.apcata.2014.04.023>

This is a PDF file of an unedited manuscript that has been accepted for publication. As a service to our customers we are providing this early version of the manuscript. The manuscript will undergo copyediting, typesetting, and review of the resulting proof before it is published in its final form. Please note that during the production process errors may be discovered which could affect the content, and all legal disclaimers that apply to the journal pertain.

A one-step method for preparation of Cu@Cu₂O nanoparticles on reduced graphene oxide and their catalytic activities in *N*-arylation of *N*-heterocycles

Siyavash Kazemi Movahed, Minoob Dabiri,* Ayoob Bazgir*

Department of Chemistry, Shahid Beheshti University, G.C. Tehran, Iran.

[Phone: +98-21-2990-3104; Fax: +98-21-2243-1661; e-mail: a_bazgir@sbu.ac.ir]

ABSTRACT

Core-shell Cu@Cu₂O nanoparticles on reduced graphene oxide (Cu@Cu₂O NPs-RGO) nanocomposite were prepared at room temperature by in situ reduction of graphene oxide (GO) and copper sulfate using *L*-ascorbic acid as reducing agent and then the air oxidation of copper nanoparticles' surface. The Cu@Cu₂O NPs-RGO nanocomposite was characterized by infrared spectroscopy, Raman spectroscopy, X-ray diffraction, X-ray photoelectron spectroscopy, transmission electron microscopy, and energy dispersive X-ray spectroscopy. Finally, Cu@Cu₂O NPs-RGO nanocomposite was used as an efficient and reusable heterogeneous catalyst in *N*-Arylation of *N*-heterocycles.

Keyword: Graphene; Copper; *N*- Arylation; Nanoparticle; *L*-Ascorbic acid

1- Introduction

The ability for efficient synthesis of *N*-arylated heterocycles is currently an active area in organic synthesis due to the prevalence of this structural motif in numerous bioactive important natural bioactive products and pharmaceutically interesting compounds [1,2]. Traditionally, *N*-arylated heterocycles have been prepared by Ullmann-type coupling of N-H containing heterocycles with aryl halides [3]. The classic Ullmann reaction normally requires harsh

conditions, such as high temperature (typically above 140 °C), stoichiometric amounts of copper and selective halide substrates, which is problematic for industrial use because of high cost and waste disposal. This protocol had other limitations such as low yields, limited scope, and lack of selectivity [4,5]. To overcome these drawbacks, a number of efforts have been made recently to develop a new catalytic system. A recent notable achievement has been the use of various copper-chelating ligands [1,6]. However, most of the successful copper-catalyzed *N*-arylation protocols suffer from serious limitations such as non-reusability of the catalysts, possible contamination of the product with metal, and usage of toxic and/or expensive ligands [7]. Ligand-free *N*-arylation reactions are rare, and generally they involve chelating substrates or they require (over)stoichiometric quantities of copper salts [8]. In principle, the use of heterogeneous catalysts could overcome some of these drawbacks mentioned above. Heterogeneous metal nanoparticles (MNPs) including CuO and Cu₂O have recently gained considerable attention because they exhibit very good activity and reusability [9,10]. In spite of their advantages, drawbacks remain in these catalysts too, as the MNPs easily agglomerate during the reaction and also less stability under severe reaction conditions, which lead to low catalytic activity as well as poor reusability of the catalyst [11]. In addition, higher stoichiometric amounts of Cu catalyst are often required. To overcome these disadvantages, anchoring the Cu catalyst onto a suitable support that would allow for the catalyst to be easily separated and recycled with minimal contamination of the product with metal is used. Recently, several different solid supports with copper anchored to their surfaces provide both the advantages of simplified isolation of the product, and easy recovery and recyclability of the catalysts [12-16]. Therefore, it is important to develop an efficient and recyclable catalyst for the *N*-arylation of heterocycles with the use of lower amounts of Cu.

Graphene has attracted great interest for its excellent mechanical, electrical, thermal and optical properties [17]. Graphene with the large theoretical specific surface area [18], high Young's modulus [19], and excellent thermal conductivity [20] and has great potential in the development of new composite materials [21], especially as a substrate to host metal and metal oxide nanoparticles [22]. Chemical reduction is the most popular strategy for the synthesis of graphene–metal nanocomposites from GO and metal salts. Hydrazine hydrate, hydroxyl-amine, and sodium borohydride are frequently used as reductants [22]. However, precautions must be taken when large quantities of these highly toxic and potentially explosive reductants are used [23,24]. Due to significant advantages of graphene, a few reports have involved the application of graphene based nanocomposites as heterogeneous catalysts in organic transformations [25].

In this work, a simple, environmentally benign, and cost effective method for the preparation of Cu@Cu₂O NPs–RGO nanocomposite by *in situ* reduction of GO and copper sulfate using *L*-ascorbic acid as an inexpensive and nontoxic reducing agent [26] with subsequent surface oxidation of Cu NPs by air is reported (Scheme 1). *L*-ascorbic acid is a very effective reducing reagent for converting copper salts to copper nanoparticles [27,28] as well as efficiently converting GO to reduced graphene oxide [26]. The Cu@Cu₂O NPs-RGO nanocomposite was used as an efficient and reusable heterogeneous catalyst for *N*-Arylation of *N*-heterocycles. Additionally, the effects of the solvent polarity, base, and temperature on yield, and recycling potential of the catalyst have all been assessed.

Scheme 1. Illustration of the synthesis procedure of Cu@Cu₂O NPs-RGO nanocomposite.

2. Experimental

2.1. Characterization

All chemicals were purchased from commercial suppliers and all solvents were purified and dried using standard procedures. IR spectra were recorded on a Bomem MB-Series FT-IR spectrophotometer. Diffraction data were collected on a STOE STADI P with scintillation detector, secondary monochromator and Cu K α radiation ($\lambda = 1.5406 \text{ \AA}$). XPS analysis was performed using a Gamdata-scienta ESCA 200 hemispherical analyzer equipped with an Al K α (1486.6 eV) X-ray source. Raman spectra were recorded on a Bruker SENTERR (2009) with an excitation beam wavelength at 785 nm. Transmission Electron Microscopy characterization of GO, Cu@Cu₂O NPs-RGO and Cu@Cu₂O NPs-RGO reused composite were performed using a transmission microscope Philips CM-30 with accelerating voltages of 150 and 250 kV. ¹H NMR spectra were recorded on a BRUKERDRX-300AVANCE spectrometer at 300.13 MHz, respectively. ¹H NMR spectra were obtained in DMSO-*d*₆ using TMS as the internal standard. Melting points of products were measured on an Electrothermal 9100 apparatus and are uncorrected. The concentration of Copper was estimated using Shimadzu AA-680 flame atomic absorption spectrophotometer. Gas chromatography was performed on a Trace GC ultra from the Thermo Company equipped with FID detector and Rtx[®]-1 capillary column.

2.2. Synthesis

2.2.1. Preparation of Graphene Oxide (GO)

The graphite powder (2.5 g) was first treated with a mixture of 12.5 ml of concentrated H₂SO₄ with 2.5 g K₂S₂O₈ and 2.5 g P₂O₅. The mixture was kept at 80 °C for 6 h. Subsequently, the mixture was cooled to room temperature and diluted with 500 mL de-ionized (DI) water and

left overnight. The mixture was then filtered and washed with DI water to remove the residual acid. The product was dried under ambient conditions overnight. The pre-oxidized graphite was then subjected to oxidation by Hummers's method. The pretreated graphite powder was put into cold (0 °C) concentrated H₂SO₄ (125 ml). Then KMnO₄ (15 g) was added gradually under stirring, and the temperature of the mixture was kept below 20 °C by cooling. The mixture was then stirred at 35 °C for 4 h and then diluted with DI water (250 ml). Because adding water to concentrated sulfuric acid medium releases a large amount of heat, the dilution was carried out in an ice bath to keep the temperature below 50 °C. After adding all of the 250 mL DI water, the mixture was stirred for 2 h, and then an additional 750 mL DI water was added. Shortly thereafter, 20 ml 30% H₂O₂ was added to the mixture and the color of the mixture changed into brilliant yellow and began bubbling. The mixture was filtered and washed with 0.1 M HCl to remove metal ions, followed by 500 mL DI water to remove the acid, and then was dialyzed against DI water. The resulting GO solid was dried in air. [29,30]

2.2.2. Preparation of Reduced Graphene Oxide (RGO)

The GO (100 mg) was ultrasonically dissolved in 20 mL of water. Then *L*-ascorbic acid (15 mmol) was gradually added into the solution and stirred for 24 h. The resulted precipitation was collected, washed with water (2 × 10 ml) and ethanol (5 × 10 ml) and dried at RT.

2.2.3. Preparation of Cu@Cu₂O NPs -RGO nanocomposite

The GO (100 mg) was ultrasonically dissolved in 20 mL of water. Then NaOH (1 mmol) was dissolved in the solution under stirring to form a uniform dispersion. After that, CuSO₄ (0.5 mmol) was added into the solution, the mixture was ultrasonically treated for 30 min. *L*-ascorbic acid (15 mmol) was gradually added into the solution and stirred for 24 h. The resulted

precipitation was collected, washed with water (5×10 ml) and Ethanol (3×10), and was exposed to air for 4h. The atomic absorption spectroscopy (AAS) analysis gave the actual Cu contents as 26.2 wt.% for Cu@Cu₂O NPs-RGO nanocomposite.

2.2.4. General procedure for *N*-Arylation of *N*-heterocycles

A mixture of Cu@Cu₂O NPs nanocomposite (5 mol % of Cu), Cs₂CO₃ (1.5 mmol), *N*-heterocycle (1.0 mmol), aryl halide (1.0 mmol), and DMSO (2 mL) under air was stirred for 1 h at 110 °C. After completion of the reaction as indicated by TLC, the heterogeneous mixture was cooled to room temperature and diluted with Ethyl acetate (10 mL). The mixture was filtered through a pad of celite. The filtrate was concentrated and then residue was purified by column chromatography (SiO₂, Ethyl acetate and *n*-Hexane) to yield pure product. The catalysts were recovered by simple filtration and washed extensively with acetone and deionized water and then drying in the air.

3. Results and discussion

3.1. Characterization of the Cu@Cu₂O NPs-RGO nanocomposite

The FT-IR spectra of GO and Cu@Cu₂O NPs-RGO are shown in Fig. 1. In the FT-IR spectroscopy of GO, the characteristic bands at 1036, 1232, 1402, 1623 and 1735 cm⁻¹ correspond to the C–O–C stretching vibrations, the C–OH stretching peak, the O–H deformation of the C–OH groups, the C=C stretching mode and the C=O stretching vibrations of the –COOH group, respectively [31]. The FT-IR spectroscopy of Cu@Cu₂O NPs-RGO nanocomposite indicate that the peak at 1735 corresponding to the stretching vibration peak of C=O disappear [32]

Fig. 1. IR spectra of GO and Cu@Cu₂O NPs-RGO nanocomposite

In the Raman spectra of GO and Cu@Cu₂O NPs-RGO nanocomposite two bands were observed around 1318 and 1592 cm⁻¹, which correspond to the disorder-induced D band and the in-phase vibration of the graphene lattice (G band) of graphene oxide, respectively (Fig. 2). The intensity ratio of D and G peaks, I(D)/I(G), is used as a measure of the disorder or restoration of the graphene lattice and expressing the sp²/sp³ carbon ratio. The I(D)/I(G) value variation is inversely proportional to the average crystallite size in graphite materials. Accordingly, while the G mode occurs at all sp² sites, the intensity of D mode is strictly connected to the presence of six-fold aromatic rings [33]. The I(D)/I(G) intensity ratio of Cu@Cu₂O NPs-RGO composite (1.49) is slightly higher than the GO (1.40) suggests a decrease in the average size of sp² domains and a high concentration of defects, possibly caused by the reduction process [34-36]. Additionally, the D band enhancement suggests interaction between the metal nanoparticles and graphene [37-41] and occurs due to the preferential growth of nanoparticles at graphene vacancies [42]. Recently, the results of atomic force microscopy (AFM) based dynamic force measurements and density functional theory based calculations shows that the interaction of the graphene surface with Cu cluster indicates the formation of charge-transfer complexes [43].

Fig. 2. Raman spectra of GO and Cu@Cu₂O NPs-RGO nanocomposite.

X-ray Diffraction (XRD) patterns of GO and Cu@Cu₂O NPs-RGO are displayed in Fig. 3a-b. It can be seen that GO showed a strong diffraction peak centered at 2θ=10.9° corresponding to the (001) interlayer spacing of 0.80 nm (Fig. 3a). In the XRD pattern of Cu@Cu₂O NPs-RGO where the major peaks at 2θ= 43.2°, 50.4°, 74.1° can be assigned to the (111), (200), (220) lattice planes of Cu (0) that are consistent with the presence of face-centred

cubic copper (JCPDS No: 4-0836) and also three minor diffraction peaks $2\theta = 36.4^\circ$, 42.4° and 61.5° can be assigned to the (111), (200) and (220) lattice planes of Cu_2O (PDF No: 01-078–2076) (Fig. 3b). An additional broad diffraction peak appears at $2\theta = 19.8\text{--}28.7^\circ$ which can be indexed to the disordered RGO sheets, with the disappearance of $2\theta = 10.9^\circ$, indicating the reduction of GO by *L*-ascorbic acid.

Fig. 3. XRD patterns a) GO and b) $\text{Cu@Cu}_2\text{O}$ NPs-RGO nanocomposite.

In order to investigate the chemical composition of the $\text{Cu@Cu}_2\text{O}$ NPs-RGO nanocomposite, XPS spectra were recorded for GO, RGO (prepared under the same method) and $\text{Cu@Cu}_2\text{O}$ NPs-RGO nanocomposite (Fig. 3). As is expected, all the three samples show a C 1s peak and O 1s peak at 284.6 and 531.3 eV, respectively (Fig. 4). The XPS survey spectrum of the $\text{Cu@Cu}_2\text{O}$ NPs-RGO nanocomposite exhibits the Cu 2p (935.0 eV) peak with its corresponding binding energy, additionally.

Fig. 4. Full range XPS spectrum of GO, RGO and $\text{Cu@Cu}_2\text{O}$ NPs-RGO nanocomposite.

The XPS spectrum of Cu 2p core level region for $\text{Cu@Cu}_2\text{O}$ NPs-RGO nanocomposite displays main peaks at 934.4 and 954.0 eV which are attributed to the binding energy of Cu $2p_{3/2}$ and Cu $2p_{1/2}$, respectively (Fig. 5). The broad Cu $2p_{3/2}$ peak has been deconvoluted into two peaks which are marked as peaks at 933.6 and 935.6 eV, and assigned to $\text{Cu}_2\text{O}/\text{Cu}$ ($\text{Cu}^{1+}/\text{Cu}^0$) and $\text{CuO}/\text{Cu}(\text{OH})_2$ (Cu^{2+}), respectively. Actually, it is difficult to differentiate Cu_2O (Cu^{1+}) and Cu^0 by the XPS feature of Cu $2p_{3/2}$ as the binding energies of Cu and Cu_2O are very close and different by only 0.1-0.2 eV. One can distinguish them from the position of their LMM auger transition in XPS spectra which are 568 eV and 570 eV for Cu and Cu_2O , respectively [44]. There is a peak at about 570.2 eV in the XPS spectra of $\text{Cu@Cu}_2\text{O}$ NPs-RGO nanocomposite.

According to above mentioned fact, one can conclude that peak at 933.6 eV is related to Cu_2O . Also, a shake-up satellite at 943.5 eV was observed in XPS spectrum. This peak is typically associated with copper in the bivalent oxidation state, which is assigned to Cu^{2+} in CuO (or probably $\text{Cu}(\text{OH})_2$ species). From these results it is inferred that the surface of copper nanoparticles is oxidized. Based on the difference between the two XRD and XPS spectra it can be reasoned that XPS only detects signals within the upper 5 nm thickness on the surface, while the XRD can detect signals in micro-order thickness [45].

Fig. 5. XPS spectrum of the Cu 2p core level region of $\text{Cu}@\text{Cu}_2\text{O}$ NPs-RGO nanocomposite.

The presence of O-containing surface functional groups was also identified by XPS measurements (Fig. 6). The broad O1s peak of GO was deconvoluted into three peaks: C=O at 530.4 eV, C(O)OH at 532.1 eV and C–OH at 533.1 eV [46]. After chemical reduction of GO by *L*-ascorbic acid, the peaks at 530.4 and 532.1 eV disappear or become weak that shows a nearly complete reduction of the GO [47]. As can be seen from XPS spectrum of the O 1s core level region of $\text{Cu}@\text{Cu}_2\text{O}$ NPs-RGO nanocomposite (Fig. 6), the presence of dominant peak at 531.3 eV, which corresponds to oxygen in metal oxides such as Cu_2O and CuO , demonstrates that the surface of copper nanoparticles is oxidized [45].

Fig. 6. XPS spectrum of the O 1s core level region of GO, RGO and $\text{Cu}@\text{Cu}_2\text{O}$ NPs-RGO nanocomposite.

A transmission electron microscopy (TEM) image of the GO displays a crumpled, layer-like structure with the size of tens of micrometers (Fig. 7a). TEM of $\text{Cu}@\text{Cu}_2\text{O}$ NPs-RGO reveals the polycrystalline nature of the nanoparticle indicating that the oxidation surface of copper nanoparticles is dispersed on the RGO sheet (Fig. 7b-d). The TEM image (Fig. 7d) of a

signal particle reveals a core-shell structure consisting of Cu₂O shell that is of *ca.* 1-2 nm thickness covering a Cu core with a 4-5 nm thickness. Additionally, Cu@Cu₂O nanoparticles are not found outside of the RGO sheets. The energy dispersive spectroscopy (EDS) of Cu@Cu₂O NPs-RGO nanocomposite in Fig. 7e clearly demonstrates the presence of Cu in the nanocomposite.

Fig. 7. (a) TEM image of GO (b-d) TEM images of Cu@Cu₂O NPs-RGO nanocomposite (e) EDS result for Cu@Cu₂O NPs-RGO nanocomposite

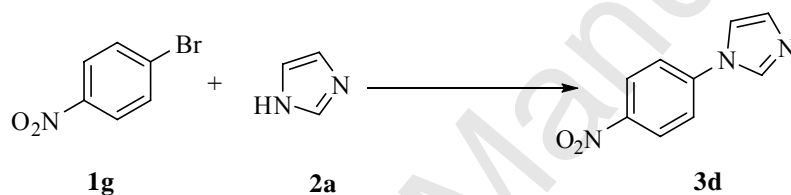
3.2. Catalytic activity toward *N*-Arylation of *N*-heterocycles

3.2.1. Effect of solvent polarity, base, and temperature

The catalytic activity of the Cu@Cu₂O NPs-RGO nanocomposite was then tested in Ullmann C-N cross-coupling of the *N*-heterocycles with aryl halides. To optimize the reaction conditions, 1-bromo-4-nitrobenzene **1g** and imidazole **2a** were selected as model substrates in the presence of various bases and solvents (Table 1). As shown in Table 1, the desired product was scarcely obtained in the presence of Cs₂CO₃ in the commonly used solvents such as CH₃CN, PhCH₃, and DMF (Table 1, entries 1-3). It was found that DMSO is the optimal solvent (Table 1, entry 4). By using DMSO as the solvent, the reaction was explored employing other bases, including K₂CO₃, K₃PO₄, and KOH (Table 1, entries 5-7). A superior yield was obtained when Cs₂CO₃ was used as the base (Table 1, entry 4). To study the effect of amount of the catalyst, the reactions were carried out at different amounts of Cu@Cu₂O NPs-RGO nanocomposite ranging from 3.5-5.0 mol% of Cu (Table 1, entries 4 and 8). It was found that when the amount of the Cu NPs-RGO increases from 3.5 to 5.0 mol %, the yields increase from 73 to 98%, respectively. It was found that 5.0 mol% Cu@Cu₂O NPs-RGO is sufficient to push forward this reaction forward (Table 1, entry 4). To optimize the reaction temperature, we also performed several

experiments at 90 °C, 100 °C, 110 °C, and 120 °C in the presence of Cs₂CO₃ in DMSO using 5.0 mol % Cu@Cu₂O NPs-RGO (Table 1, entries 4 and 10-12). As can be seen from Table 1, the optimal reaction temperature is 110 °C (Table 1, entry 4). It is also noteworthy that, when this reaction was carried out with GO or RGO, we failed to isolate any coupled product (entries 13 and 14). Additionally, Cu@Cu₂O-Activated Carbon was tested and exhibited middle catalytic activity.

Table 1. Screening of the reaction conditions^a



Entry	Solvent	Base	Temp. (°C)	Time (h)	Conversion (%) ^b	Yield (%) ^c
1	CH ₃ CN	Cs ₂ CO ₃	Reflux	10	31	27
2	PhCH ₃	Cs ₂ CO ₃	Reflux	24	Trace	Trace
3	DMF	Cs ₂ CO ₃	110	10	57	52
4	DMSO	Cs ₂ CO ₃	110	1	100	98
5	DMSO	K ₂ CO ₃	110	2	69	62
6	DMSO	K ₃ PO ₄	110	2	92	84
7	DMSO	KOH	110	2	60	53
8 ^d	DMSO	Cs ₂ CO ₃	110	1	81	73
9	DMSO	Cs ₂ CO ₃	90	1	76	71
10	DMSO	Cs ₂ CO ₃	100	1	91	87
11	DMSO	Cs ₂ CO ₃	120	1	100	98

12 ^e	DMSO	Cs ₂ CO ₃	110	1	n. r.	n. r.
13 ^f	DMSO	Cs ₂ CO ₃	110	1	n. r.	n. r.
15 ^g	DMSO	Cs ₂ CO ₃	110	1	65	57

^a 1-bromo-4-nitrobenzene (0.5 mmol), imidazole (0.5 mmol), Base (0.75 mmol), and Cu@Cu₂O NPs-RGO nanocomposite (5.0 mol% of Cu).

^b Conversion determined by gas chromatography based on arylhalide and *n*-dodecane was used as an internal standard

^c Isolated yield

^d Cu@Cu₂O NPs-RGO nanocomposite (3.5 mol% of Cu).

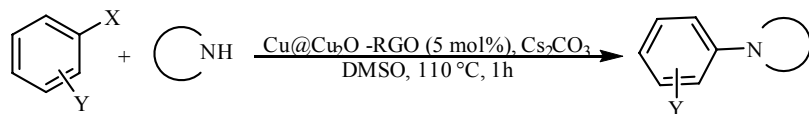
^e GO (100 mg)

^f RGO (100 mg)

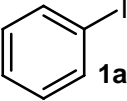
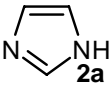
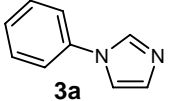
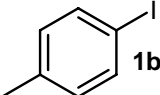
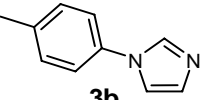
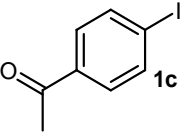
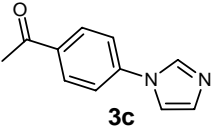
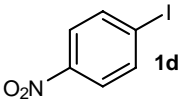
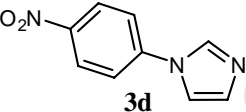
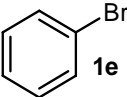
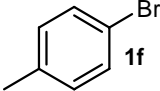
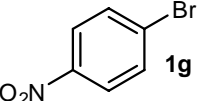
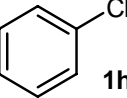
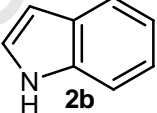
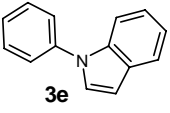
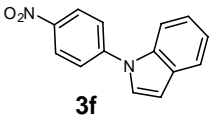
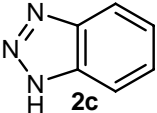
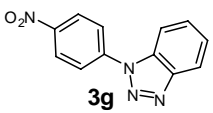
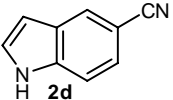
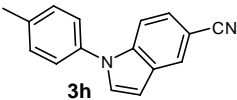
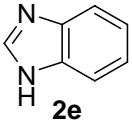
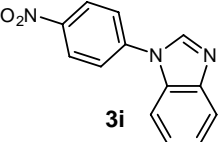
^g Cu@Cu₂O-Activated Carbon (5.0 mol% of Cu).

After determining the optimized conditions, we then investigated the scope of the Cu@Cu₂O NPs-RGO nanocomposite for the C–N cross-coupling reaction of a variety of aryl halides with imidazole (Table 2). The *N*-arylation of imidazole with aryl iodides and aryl bromides bearing electron-donating and electron-withdrawing groups was done effectively and gave good yields (Table 2, entries 1-4 and 6-5). Under these conditions, chlorobenzene show less reactivity as compared to bromobenzene and iodobenzene (entry 8). The reactivity of different aryl halides is ArI > ArBr > ArCl. Other *N*-heterocycles such as benzimidazole, benzotriazole and indole reacted with aryl bromides under standard experimental conditions and provided products with 83-94% yields (Table 3, entries 9-13).

Table 2. Cu@Cu₂O NPs-RGO nanocomposie catalyzed *N*-arylation of *N*-heterocycles



Accepted Manuscript

1				100	96
2		2a		100	96
3		2a		100	98
4		2a		100	98
5		2a	3a	95	92
6		2a	3b	100	94
7		2a	3d	100	98
8		2a	3a	64	56
9	1e			93	90
10	1g	2b		93	87
11	1g			88	83
12	1f			100	94
13	1g			89	

^c Conversion determined by gas chromatography based on arylhalide, *n*-dodecane was used as an internal standard

^b Isolated yield

Table 3, compares efficiency of Cu@Cu₂O NPs-RGO nanocomposite (reaction conditions, yield and time) with efficiency of other reported heterogeneous copper catalysts in Ullmann C-N cross-coupling. It is clear from Table 3 that our method is simpler, and less time consuming for *N*-arylation of *N*-heterocycles with aryl bromides.

Table 3. Comparison of efficiency of various heterogeneous copper catalysts in *N*-arylation of *N*-heterocycles with aryl bromides

Catalyst	Condition	Yield (%)	Time (h)	Ref.
Cu@Cu ₂ O NP-RGO (5 mol%)	Cs ₂ CO ₃ , DMSO, 110 °C	83-98	1	This work
CuFAP (12.5 mol%)	K ₂ CO ₃ , DMSO, 110 °C	85-98	4-15	48
CuO/MWCNT (0.98 mol%)	K ₂ CO ₃ , DMAc, 120 °C	96-47	24	13
CuI/MNP-3 (10 mol%)	Cs ₂ CO ₃ , DMF, 110 °C	30-98	24	49
Activated-Cu (10 mol%)	LiOH, TBAB, H ₂ O, 120 °C	35-81	24	50

3.2.2. Recycling the Cu@Cu₂O NPs-RGO composite

The X-ray Diffraction (XRD) pattern Cu@Cu₂O NPs-RGO after five runs is shown in Fig. 9. The peaks of Cu and Cu₂O phases can be easily observed.

Fig. 8. XRD pattern of Cu@Cu₂O NPs-RGO nanocomposite after five runs used

TEM image of the Cu@Cu₂O NPs-RGO composite after five runs is showed in Fig. 10 indicating the more oxidation surface of copper nanoparticles.

Fig. 9. TEM image of Cu@Cu₂O NPs-RGO nanocomposite after five runs used.

The XPS spectrum of Cu 2p core level region for Cu@Cu₂O NPs-RGO nanocomposite after five runs used displays main peaks at 933.9 and 953.8 eV which are attributed to the binding energy of Cu 2p_{3/2} and Cu 2p_{1/2}, respectively (Fig. 11). The broad Cu 2p_{3/2} peak has been deconvoluted into two peaks which are marked as peaks at 933.6 and 934.5 eV, and assigned to Cu₂O/Cu (Cu¹⁺/Cu⁰) and CuO/Cu(OH)₂ (Cu²⁺), respectively. By integrating the area in the XPS has been found the ratio of Cu₂O/Cu (Cu¹⁺/Cu⁰): CuO/Cu(OH)₂ (Cu²⁺) to be 3:7 (than this ratio for fresh nanocomposite 6:4) that indicated more oxidation surface of Cu@Cu₂O nanoparticles. Binding energy of Cu 2p_{3/2} of the used nanocomposite is 933.9 eV (Fig. 10), which has -0.5 eV difference from Cu@Cu₂O species of the fresh catalyst (Fig. 5). This illustrates that the Cu@Cu₂O nanoparticles surfaces have adsorbed or chelated with some anions such as Br⁻, CO₃²⁻ in reaction mixture [16].

Fig. 10. XPS spectrum of the Cu 2p core level region of Cu@Cu₂O NPs-RGO nanocomposite after five runs used.

3.2.3. Hot filtration test and AAS analysis

The heterogeneous nature of the catalysis was proved using a hot filtration test and AAS analysis. To determine whether the catalyst is actually functioning in a heterogeneous manner or whether it is merely a reservoir for more active soluble copper species, a hot filtration test was performed in the C-N cross-coupling of bromobenzene with imidazole after ~50% of the coupling reaction is completed. The hot filtrates were then transferred to another flask containing Cs₂CO₃ (1.5 equiv.) in DMSO (2 mL) at 110 °C. Upon the further heating of catalyst-free solution for 2 h, no considerable progress (~7% by GC analysis) was observed. Then, the possibility of Cu leakage from Cu@Cu₂O NPs-RGO nanocomposite to the medium during the

reaction was investigated (Table 4). AAS results of the used Cu@Cu₂O NPs-RGO nanocomposite catalyst indicate leaching of 0.9% of copper in the *N*-arylation reaction of bromobenzene with imidazole after the first cycle and 6.1% after the fifth cycle.

Table 4. Reusability of Cu@Cu₂O NPs-RGO nanocomposite and leaching of Cu in multi-cycle *N*-arylation reactions

Cycle	Product yield ^a (%)	Leaching of Cu (%)
1	92	0.9
2	91	1.3
3	87	1.2
4	83	1.4
5	75	1.3

^a Reaction conditions: bromobenzene (0.5 mmol), imidazole (0.5 mmol), Cs₂CO₃ (0.75 mmol), and Cu@Cu₂O NPs-RGO nanocomposite (5.0 mol% of Cu) (for cycle 1 and the remaining recovered amount of the catalyst was used for subsequent cycles), DMSO (2 mL), 1 h, 110 °C.

To determine the reproducibility of the catalyst, we applied the same batch of catalyst and also two different batches of catalyst for replicate experiments, this was checked by repeating the runs at least three times on the same batch of catalyst and for another three times of two different batches of catalyst for *N*-arylation of imidazole by bromobenzene. These results were found to be within acceptable limits ($\pm 1\%$ for the same batch of the catalyst and $\pm 3\%$ for different batches of the catalyst).

4. Conclusions

In conclusion, we have demonstrated for the first time that Cu@Cu₂O NPs-RGO nanocomposite is an effective and reusable heterogeneous catalyst for the Ullmann C-N cross-coupling reaction with good yields under aerobic conditions for a short reaction times without using any external ligands or an additives as promoters. The catalyst was recovered by simple filtration and reused for several cycles.

Acknowledgements

We gratefully acknowledge financial support from the Research Council of Shahid Beheshti University.

References

- [1] G. Evano, N. Blanchard, M. Toumi, *Chem. Rev.* 108 (2008) 3054-3131.
- [2] Negwer, M. In *Organic-Chemical Drugs and their Synonyms*, 8th ed.; VCH-Wiley: Berlin, 2002.
- [3] Hassan, J, Sevignon, M, Gozzi, C, Schulz, E, Lemaire, M. *Chem. Rev.* 102 (2002) 1359–1469.
- [4] F. Ullmann, *Ber. Dtsch. Chem. Ges.* 36 (1903) 2382-2384.
- [5] F. Ullmann, *Ber. Dtsch. Chem. Ges.* 37 (1904) 853-854.
- [6] I. P. Beletskaya, A. V. Cheprakov *Coord. Chem. Rev.* 248 (2004) 2337–2364.
- [7] M. L. Kantam, M. Roy, S. Roy, B. Sreedhara, R. L. De, *Catal. Commun.* 9 (2008) 2226-2230.
- [8] A. Correa, C. Bolm, *Adv. Synth. Catal.* 349 (2007) 2673–2676.
- [9] S. Ganesh Babu, R. Karvembu, *Ind. Eng. Chem. Res.* 50 (2011) 9594–9600.

- [10] M. L. Kantam, Y. Jagjit, L. Soumi, S. Bojja, J. Shailendra, *Adv. Synth. Catal.* 349 (2007) 1938–1942.
- [11] S. Mandal, D. Roy, R. V. Chaudhari, M. Sastry, *Chem. Mater.* 16 (2004) 3714–3724.
- [12] M. L. Kantam, J. Yadav, S. Laha, B. Sreedhar, S. Jha, *Adv. Synth. Catal.* 349 (2007) 1938–1942.
- [13] M. Gopiraman, S. G. Babu, Z. Khatri, W. Kai, Y. A. Kim, M. Endo, R. Karvembu, I. S. Kim, *Carbon* 62 (2013) 135–148.
- [14] A. Y. Kim, H. J. Lee, J. C. Park, H. Kang, H. Yang, H. Song, K. H. Park *Molecules* 14 (2009) 5169-5178.
- [15] S.U. Son, I.K. Park, J. Park, T. Hyeon, *Chem. Commun.* (2004) 778-779.
- [16] Z. Huang, F. Li, B. Chen, F. Xue, G. Chen, G. Yuan *Appl. Catal. A* 403 (2011) 104–111
- [17] X. Huang, Z. Yin, S. Wu, X. Qi, Q. He, Q. Zhang, Q. Yan, F. Boey, H. Zhang, *Small* 7 (2011) 1876-1902.
- [18] M.D. Stoller, S. Park, Y. Zhu, J. An, R.S. Ruoff, *Nano Lett.* 8 (2008) 3498-3502.
- [19] C. Lee, X.D. Wei, J.W. Kysar, J. Hone, *Science* 321 (2008) 385-388.
- [20] A.A. Balandin, S. Ghosh, W. Bao, I. Calizo, D. Teweldebrhan, F. Miao, C.N. Lau, *Nano Lett.* 8 (2008) 902-907.
- [21] H.M.A. Hassan, V. Abdelsayed, A.E.R.S. Khder, K.M. AbouZeid, J. Turner, M.S. El-Shall, S.I. Al-Resayes, A.A. El-Azhary, *J. Mater. Chem.* 19 (2009) 3832-3837.
- [22] R.X. Huang, X. Qi, F. Boey, H. Zhang, *Chem. Soc. Rev.* (2012) 666-686.

- [23] A. Furst, R. C. Berlo and S. Hooton, *Chem. Rev.* 65 (1965) 51–68.
- [24] P. Raveendran, J. Fu, S. L. Wallen, *J. Am. Chem. Soc.* 125 (2003) 13940–13941
- [25] S. Bai, X. Shen, *RSC Advances* 2 (2012) 64-98.
- [26] J. Zhang, H. Yang, G. Shen, P. Cheng, J. Zhang, S. Guo *Chem. Commun.* 46 (2010) 1112–1114.
- [27] J. Xiong, Y. Wang, Q. Xue, X. Wu *Green Chem.* 13 (2011) 900–904.
- [28] M Biçer, İ Şişman *Powder Technol.* 198 (2010) 279–284.
- [29] W.S. Hummers, R.E. Offeman *J. Am. Chem. Soc.* 80 (1958) 1339-1339.
- [30] N.I. Kovtyukhova, P.J. Olliver, B.R. Martin, T.E. Mallouk, S.A.Chizhik, E.V. Buzaneva, A.D. Gorchinsky *Chem. Mater.* 11 (1999) 771-778.
- [31] H. T. Hu, X. B. Wang, F. M. Liu, J. C. Wang, C. H. Xu, *Synth. Met.* 161 (2011) 404–410.
- [32] P. Dong, Y. Wang, L. Guo, B. Liu, S. Xin, J. Zhang, Y. Shi, W. Zeng, S. Yin *Nanoscale* 4 (2012) 4641–4649.
- [33] A. C. Ferrari, J. Robertson, *Phys. Rev. B* 61 (2000) 14095–14107.
- [34] S. Cui, Z. Wen, E. C. Mattson, S. Mao, J. Chang, M. Weinert, C. J. Hirschmugl, M. Gajdardziska-Josifovska, J. Chen, *J. Mater. Chem. A* 1 (2013) 1 4462-4467.
- [35] Z.-G. Le, Z. Liu, Y. Qian, C. Wang, *Appl. Surf. Sci.* 258 (2012) 5348-5353.
- [36] S. Stankovich, D. A. Dikin, R. D. Piner, K. A. Kohlhaas, A. Kleinhammes, Y. Jia, Y. Wu, S. T. Nguyen, R. S. Ruoff, *Carbon* 45 (2007) 1558-1565.
- [37] K. Jasuja, V. Berry, *ACS Nano* 3 (2009) 2358-2366.

- [38] K. Jasuja, J. Linn, S. Melton, V. Berry, J. Phys. Chem. Lett. 1 (2010) 1853-1860.
- [39] Y. Li, X. Fan, J. Qi, J. Ji, S. Wang, G. Zhang, F. Zhang, Nano Res. 3 (2010) 429-437.
- [40] M. Fu, Q. Jiao, Y. Zhao, J. Mater. Chem. A, 1 (2013) 5577–5586.
- [41] S. Cui, Z. Wen, E. C. Mattson, S. Mao, J. Chang, M. Weinert, C. J. Hirschmugl, M. Gajdardziska-Josifovska, J. Chen, J. Mater. Chem. A, 1 (2013) 4462–4467.
- [42] M. Iliut, C. Leordean, V. Canpean, C.-M. Teodorescu, S. Astilean J. Mater. Chem. C 1 (2013) 4094-4104
- [43] P. Lazar, S. Zhang, K. Safarova, Q. Li, J. P. Froning, J. Granatier, P. Hobza, R. Zboril, F. Besenbacher, M. Dong, M. Otyepka, ACS Nano 7 (2013) 1646–1651.
- [44] T. Ghodselahi, M.A. Vesaghi, A. Shafiekhani, A. Baghizadeh, M. Lameii Appl. Surf. Sci. 255 (2008) 2730-2734.
- [45] Z. Ai, L. Zhang, S. Lee, W. Ho J. Phys. Chem. C 113 (2009) 20896-20902.
- [46] O. Akhavan Carbon 48 (2010) 509–519
- [47] Y. Wang, S. Zhang, D. Du, Y. Shao, Z. Li, J. Wang, M. H. Engelhard, J. Li, Y. Lin. J. Mater. Chem. 21 (2011) 5319-5325.
- [48] M. L. Kantam, G. T. Venkanna, Ch. Sridhar, K. B. S. Kumar, Tetrahedron Lett. 47 (2006) 3897–3899
- [48] G. Chouhan, D. Wang, H. Alper, Chem. Commun. (2007) 4809–4811.
- [49] Q. Yang, Y. Wang, D. Lina, M. Zhang Tetrahedron Lett. 54 (2013) 1994–1997.

Figure captions

Fig. 1. IR spectra of GO and Cu@Cu₂O NPs-RGO nanocomposite

Fig. 2. Raman spectra of GO and Cu@Cu₂O NPs-RGO nanocomposite.

Fig. 3. XRD patterns a) GO and b) Cu@Cu₂O NPs-RGO nanocomposite.

Fig. 4. Full range XPS spectrum of GO, RGO and Cu@Cu₂O NPs-RGO nanocomposite.

Fig. 5. XPS spectrum of the Cu 2p core level region of Cu@Cu₂O NPs-RGO nanocomposite.

Fig. 6. XPS spectrum of the O 1s core level region of GO, RGO and Cu@Cu₂O NPs-RGO nanocomposite.

Fig. 7. (a) TEM image of GO (b-d) TEM images of Cu@Cu₂O NPs-RGO nanocomposite (e) EDS result for Cu@Cu₂O NPs-RGO nanocomposite.

Fig. 8. XRD pattern of Cu@Cu₂O NPs-RGO nanocomposite after five runs used.

Fig. 9. TEM image of Cu@Cu₂O NPs-RGO nanocomposite after five runs used.

Fig. 10. XPS spectrum of the Cu 2p core level region of Cu@Cu₂O NPs-RGO nanocomposite after five runs used.

Table captions

Table 1. Screening of the reaction conditions

Table 2. Cu@Cu₂O NPs-RGO catalyzed *N*-arylation of *N*-heterocycles

Table 3. Comparison of efficiency of various heterogeneous copper catalysts in *N*-arylation of *N*-heterocycles with aryl bromides

Table 4. Reusability of Cu@Cu₂O NPs-RGO nanocomposite and leaching of Cu in multi-cycle *N*-arylation reactions

Scheme caption

Scheme 1. Illustration of the synthesis procedure of Cu@Cu₂O NPs-RGO nanocomposite.

Accepted Manuscript

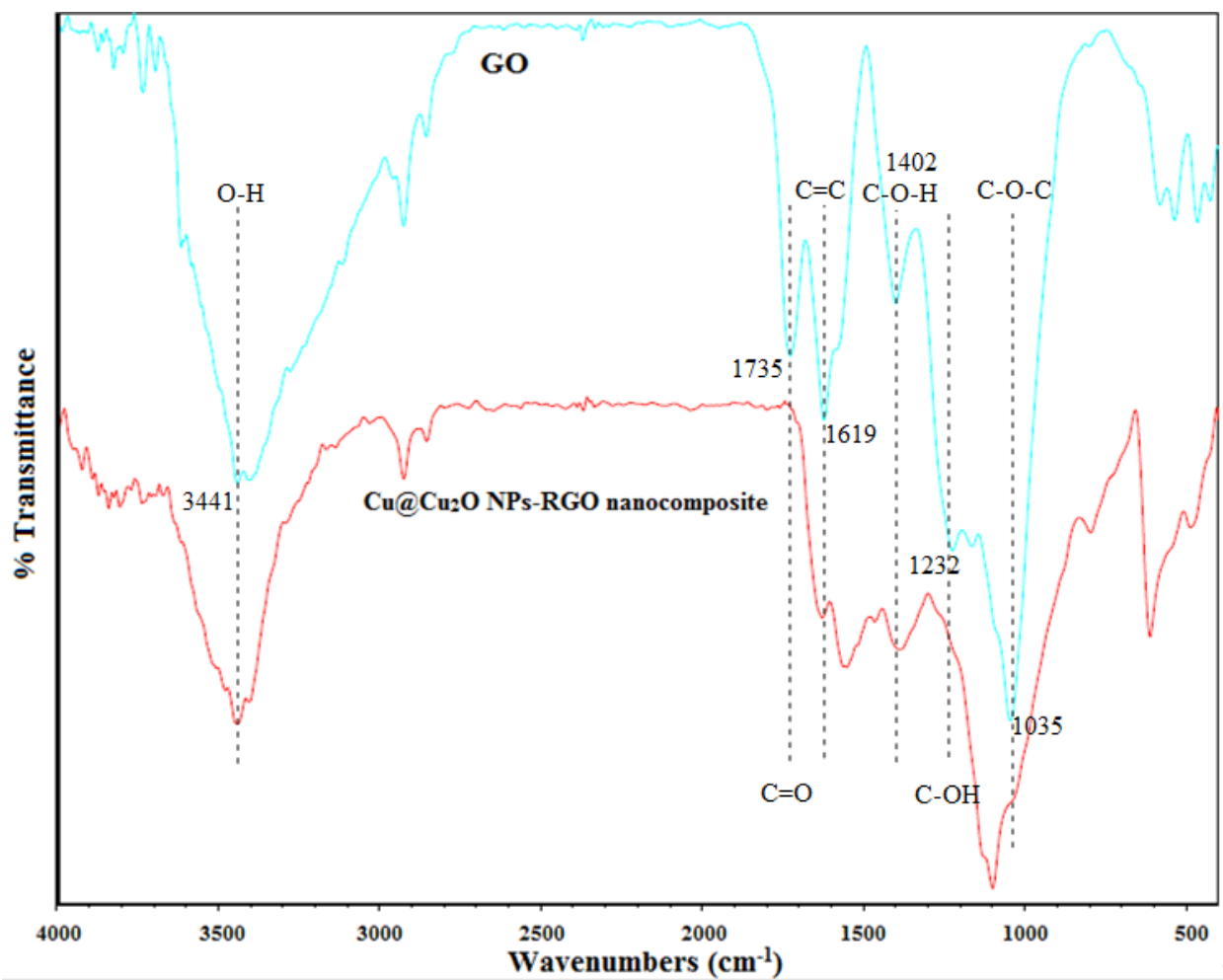


Fig. 1. IR spectra of GO and Cu@Cu₂O NPs-RGO nanocomposite

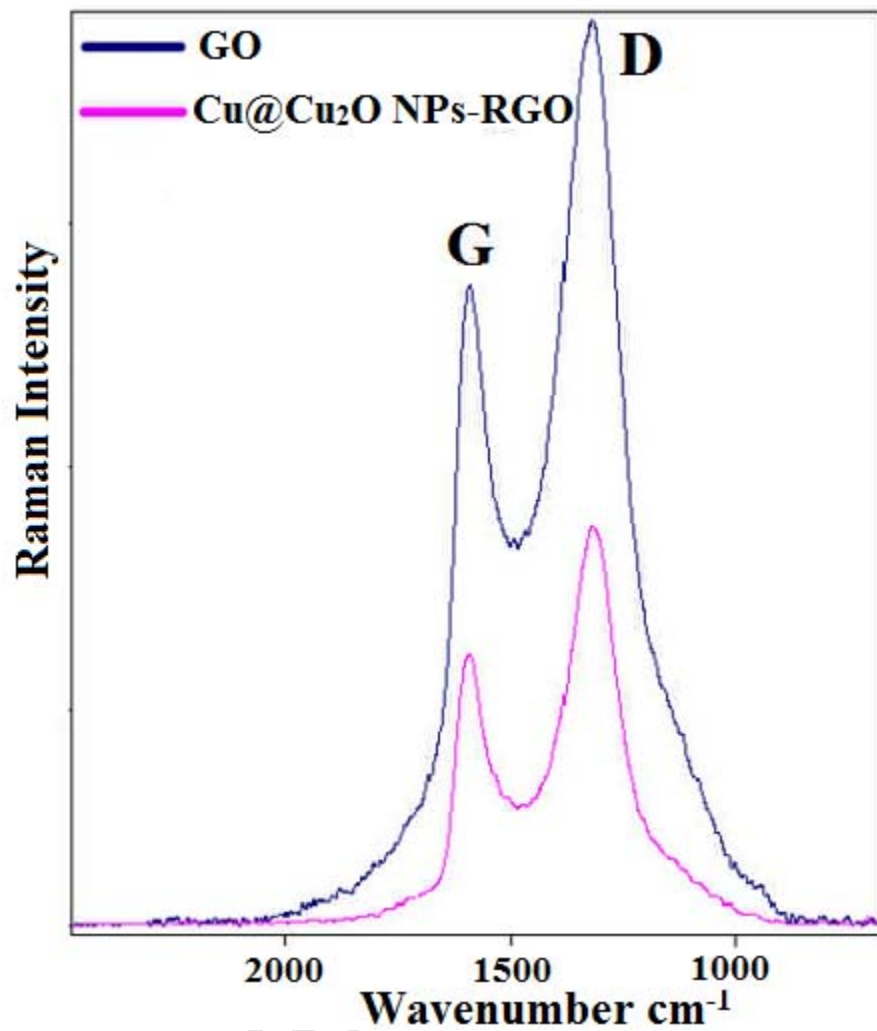


Fig. 2. Raman spectra of GO and Cu@Cu₂O NPs-RGO nanocomposite.

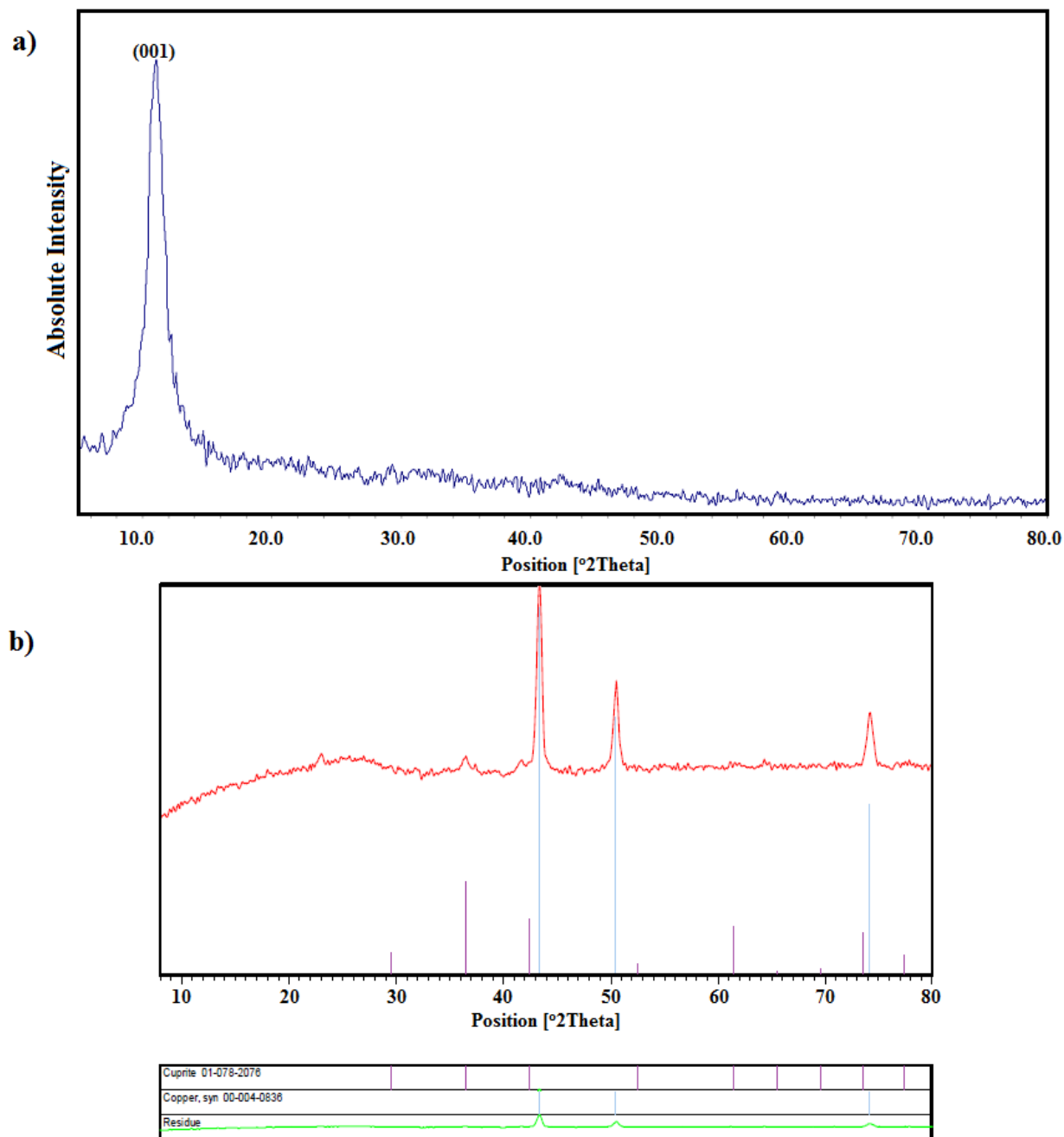


Fig. 3. XRD patterns a) GO and b) Cu@Cu₂O NPs-RGO nanocomposite.

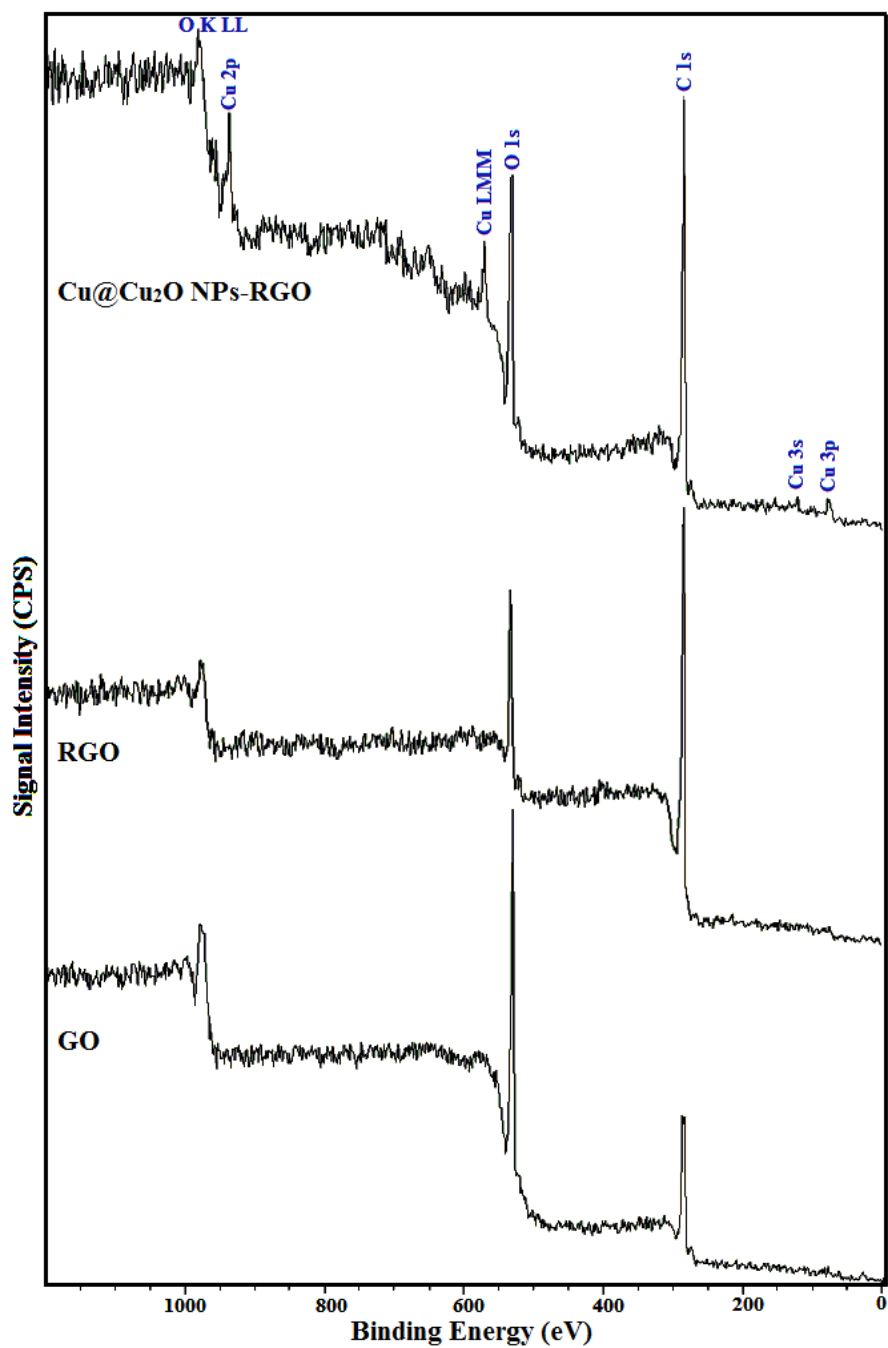


Fig. 4. Full range XPS spectrum of GO, RGO and Cu@Cu₂O NPs-RGO nanocomposite.

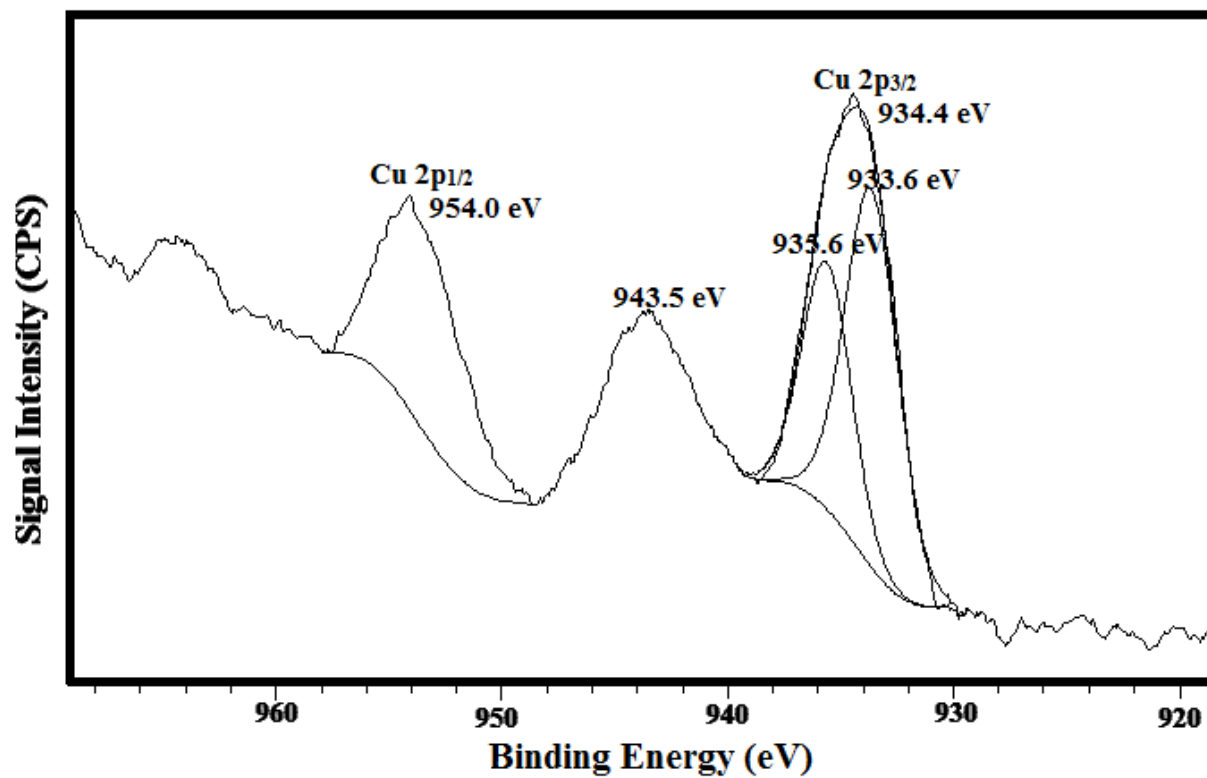


Fig. 5. XPS spectrum of the Cu 2p core level region of Cu@Cu₂O NPs-RGO nanocomposite.

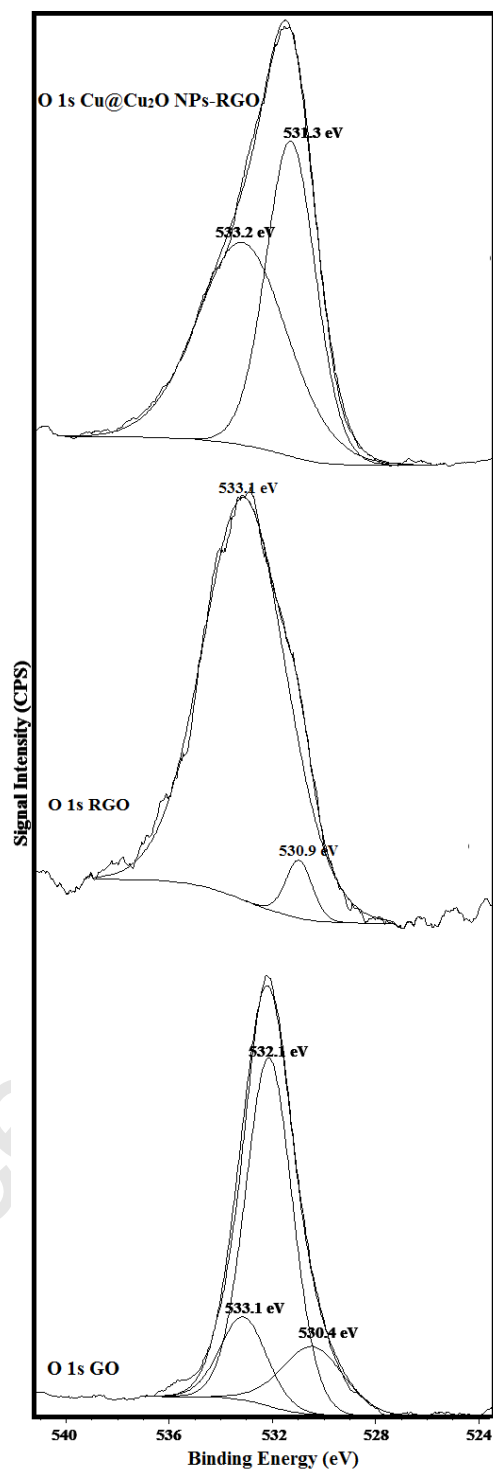


Fig. 6. XPS spectrum of the O 1s core level region of GO, RGO and Cu@Cu₂O NPs-RGO nanocomposite.

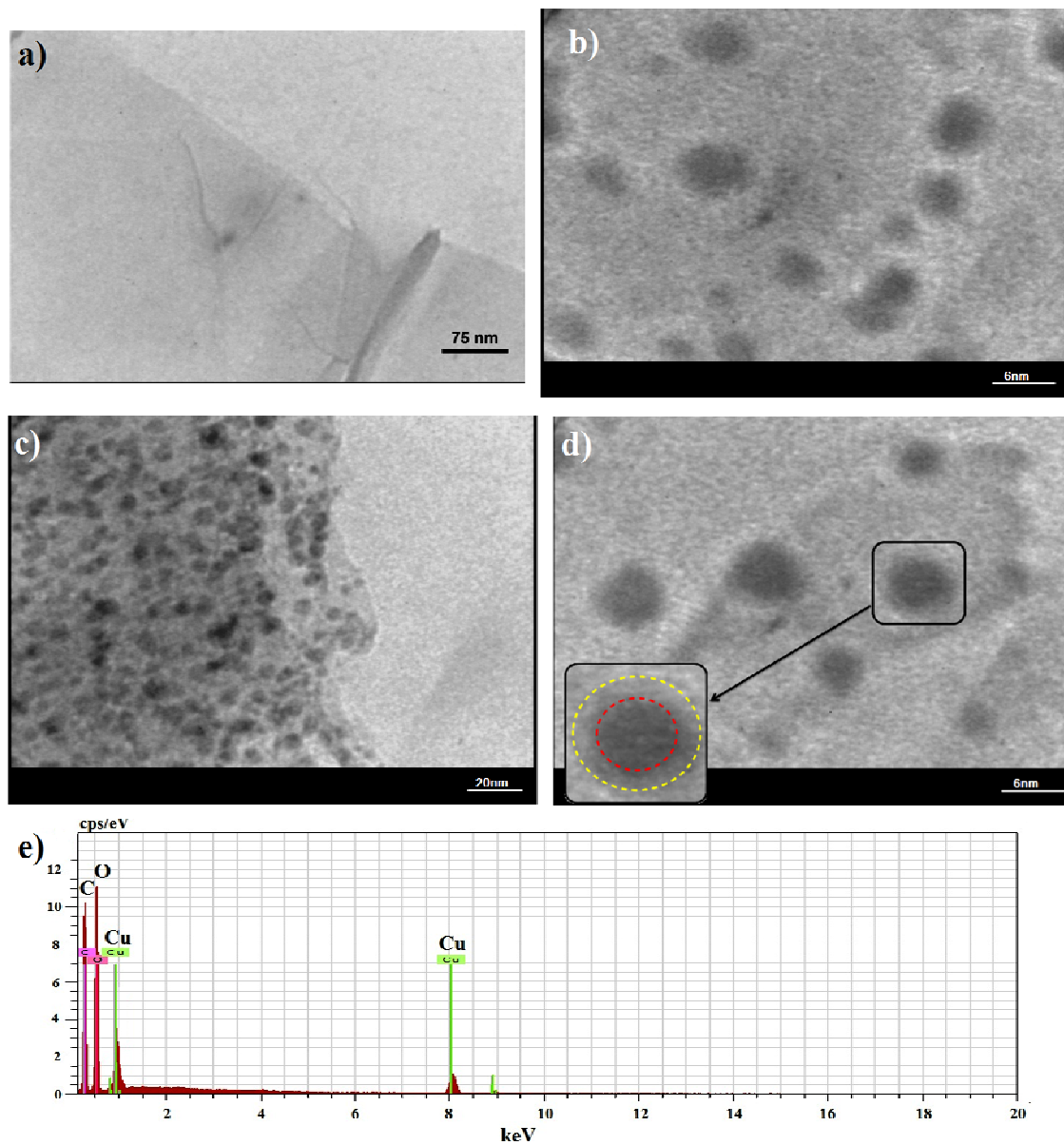


Fig. 7. (a) TEM image of GO (b-d) TEM images of Cu@Cu₂O NPs-RGO nanocomposite (e) EDS result for Cu@Cu₂O NPs-RGO nanocomposite.

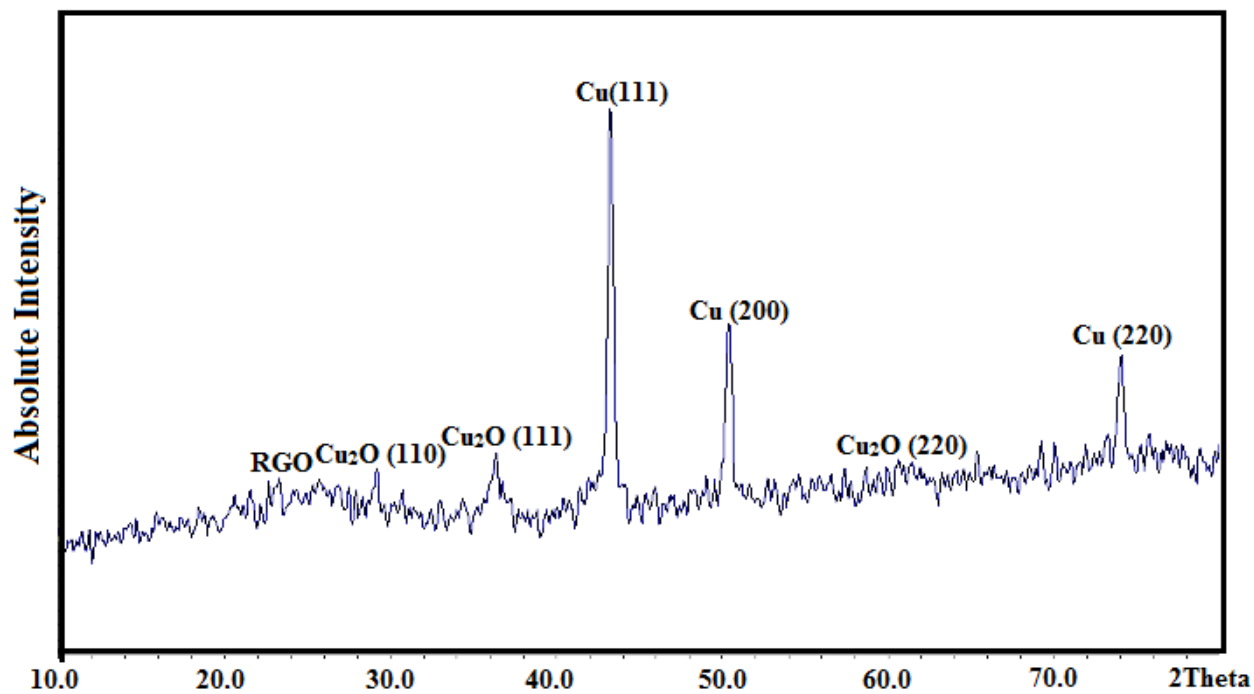


Fig. 8. XRD pattern of Cu@Cu₂O NPs-RGO nanocomposite after five runs used.

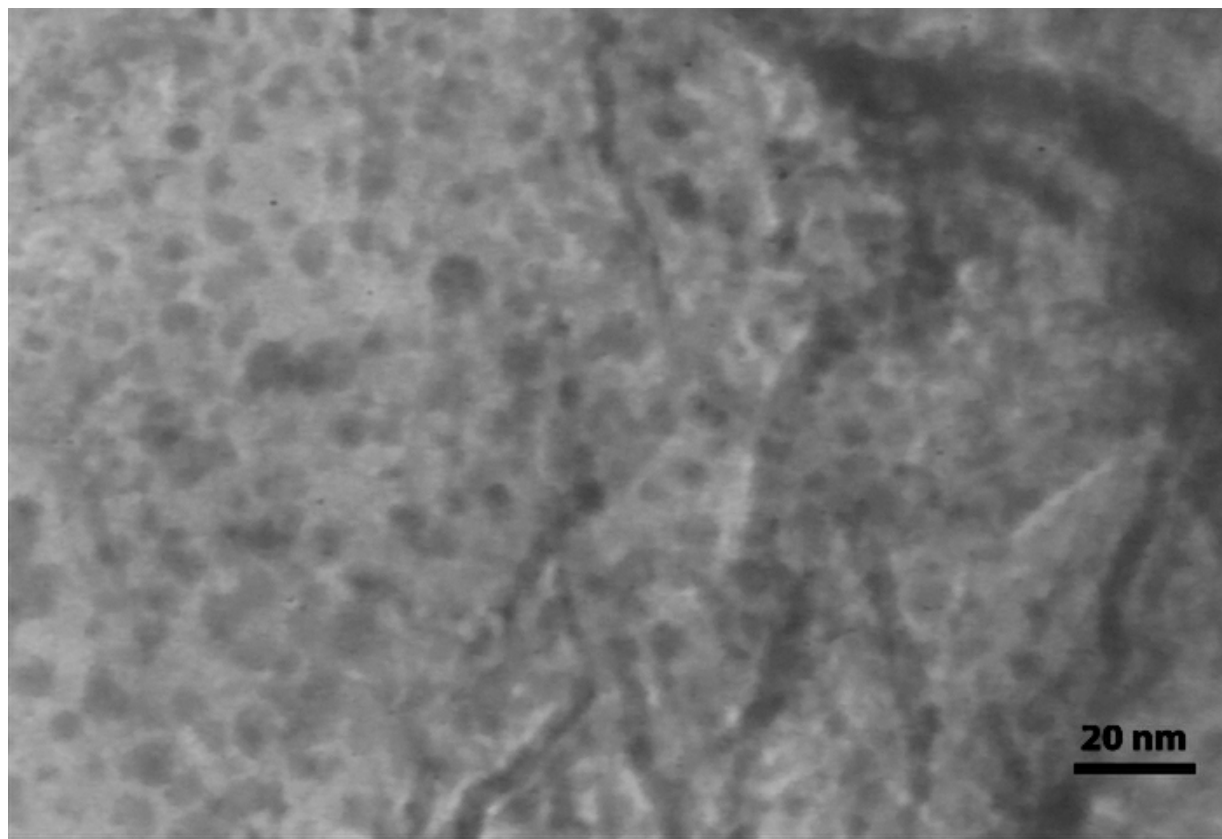


Fig. 9. TEM image of Cu@Cu₂O NPs-RGO nanocomposite five runs used.

Accepted

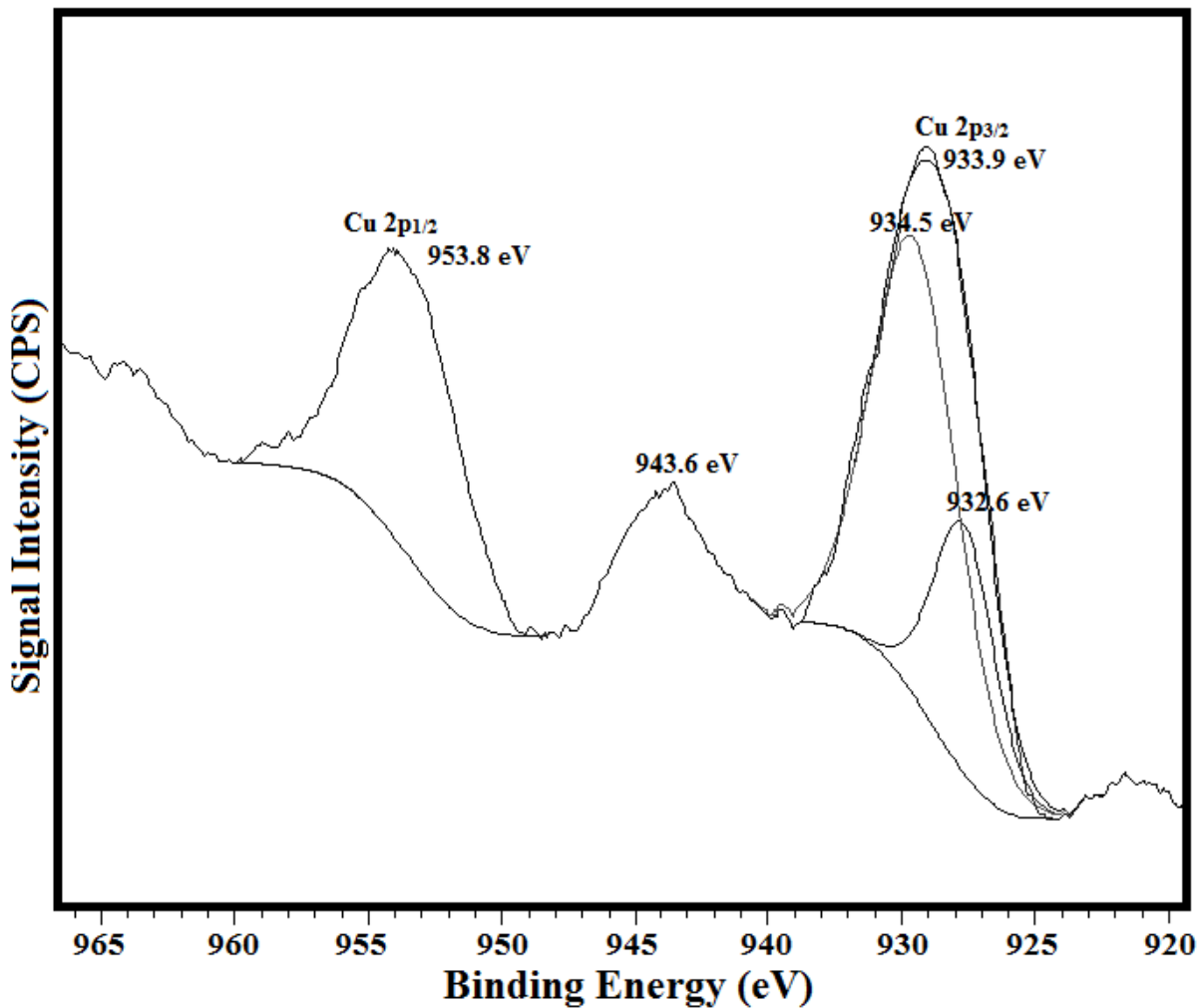
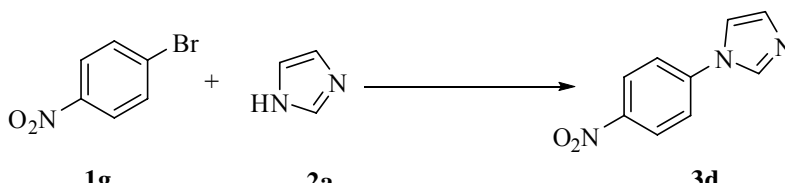


Fig. 10. XPS spectrum of the Cu 2p core level region of Cu@Cu₂O NPs-RGO nanocomposite five runs used.

Table 1. Screening of the reaction conditions^a


Entry	Solvent	Base	Temp. (°C)	Time (h)	Conversion (%) ^b	Yield (%) ^c
1	CH ₃ CN	Cs ₂ CO ₃	Reflux	10	31	27
2	PhCH ₃	Cs ₂ CO ₃	Reflux	24	Trace	Trace
3	DMF	Cs ₂ CO ₃	110	10	57	52
4	DMSO	Cs ₂ CO ₃	110	1	100	98
5	DMSO	K ₂ CO ₃	110	2	69	62
6	DMSO	K ₃ PO ₄	110	2	92	84
7	DMSO	KOH	110	2	60	53
8 ^d	DMSO	Cs ₂ CO ₃	110	1	81	73
9	DMSO	Cs ₂ CO ₃	90	1	76	71
10	DMSO	Cs ₂ CO ₃	100	1	91	87
11	DMSO	Cs ₂ CO ₃	120	1	100	98
12 ^e	DMSO	Cs ₂ CO ₃	110	1	n. r.	n. r.
13 ^f	DMSO	Cs ₂ CO ₃	110	1	n. r.	n. r.
15 ^g	DMSO	Cs ₂ CO ₃	110	1	65	57

^a 1-bromo-4-nitrobenzene (0.5 mmol), imidazole (0.5 mmol), Base (0.75 mmol), and Cu@Cu₂O NPs-RGO nanocomposite (5.0 mol% of Cu).

^b Conversion determined by gas chromatography based on arylhalide and *n*-dodecane was used as an internal standard

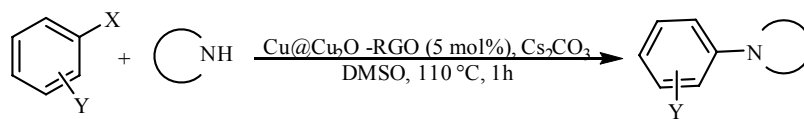
^c Isolated yield

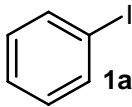
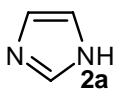
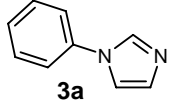
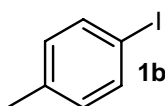
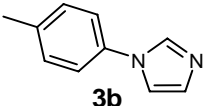
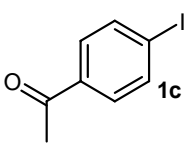
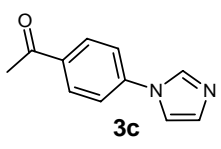
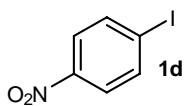
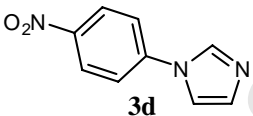
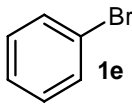
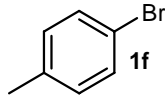
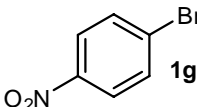
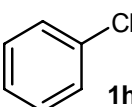
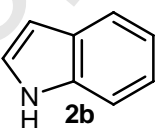
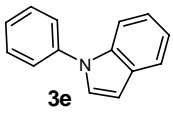
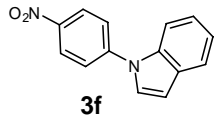
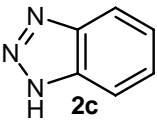
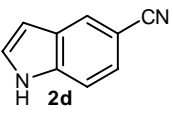
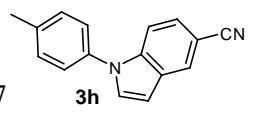
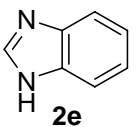
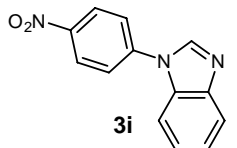
^d Cu@Cu₂O NPs-RGO nanocomposite (3.5 mol% of Cu).

^e GO (100 mg)

^f RGO (100 mg)

^g Cu@Cu₂O-Activated Carbon (5.0 mol% of Cu).

Table 2. Cu@Cu₂O NPs-RGO nanocomposite catalyzed *N*-arylation of *N*-heterocycles

1				100	96
2		2a		100	96
3		2a		100	98
4		2a		100	98
5		2a	3a	95	92
6		2a	3b	100	94
7		2a	3d	100	98
8		2a	3a	64	56
9	1e			93	90
10	1g	2b		93	87
11	1g			88	83
12	1f			100	94
13	1g			89	

^c Conversion determined by gas chromatography based on arylhalide, *n*-dodecane was used as an internal standard

^b Isolated yield

Accepted Manuscript

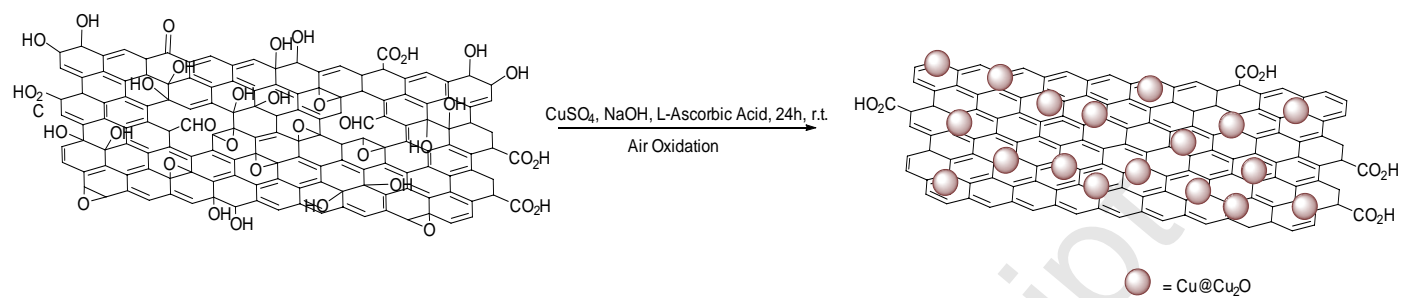
Table 3. Comparison of efficiency of various heterogeneous copper catalysts in *N*-arylation of *N*-heterocycles with aryl bromides

Catalyst	Condition	Yield (%)	Time (h)	Ref.
Cu@Cu ₂ O NP-RGO (5 mol%)	Cs ₂ CO ₃ , DMSO, 110 °C	83-98	1	This work
CuFAP (12.5 mol%)	K ₂ CO ₃ , DMSO, 110 °C	85-98	4-15	48
CuO/MWCNT (0.98 mol%)	K ₂ CO ₃ , DMAc, 120 °C	96-47	24	13
CuI/MNP-3 (10 mol%)	Cs ₂ CO ₃ , DMF, 110 °C	30-98	24	49
Activated-Cu (10 mol%)	LiOH, TBAB, H ₂ O, 120 °C	35-81	24	50

Table 4. Reusability of Cu@Cu₂O NPs-RGO nanocomposite and leaching of Cu in multi-cycle *N*-arylation reactions

Cycle	Product yield ^a (%)	Leaching of Cu (%)
1	92	0.9
2	91	1.3
3	87	1.2
4	83	1.4
5	75	1.3

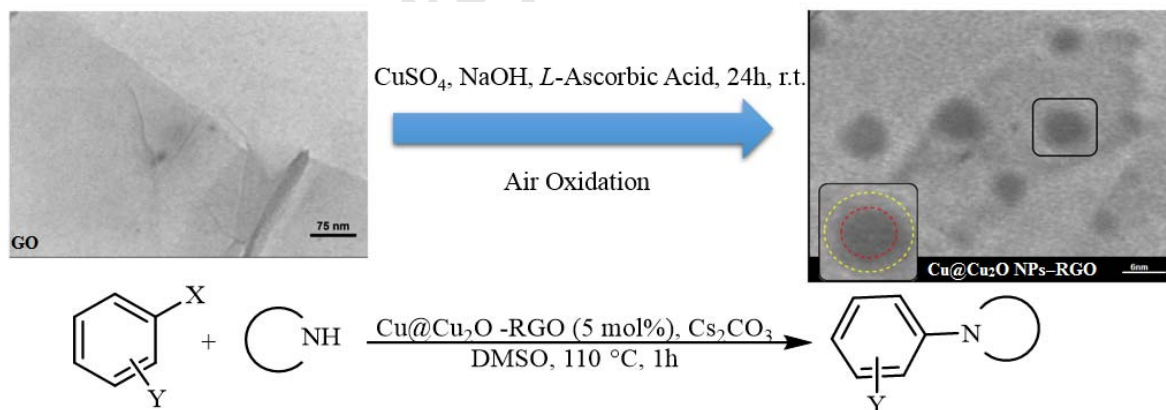
^a Reaction conditions: bromobenzene (0.5 mmol), imidazole (0.5 mmol), Cs₂CO₃ (0.75 mmol), and Cu@Cu₂O NPs-RGO nanocomposite (5.0 mol% of Cu) (for cycle 1 and the remaining recovered amount of the catalyst was used for subsequent cycles), DMSO (2 mL), 1 h, 110 °C.



Scheme 1. Illustration of the synthesis procedure of Cu@Cu₂O NPs-RGO nanocomposite.

A one-step method to preparation of Cu@Cu₂O nanoparticles on reduced graphene oxide and their catalytic activities for *N*-arylation of *N*-heterocyclic compounds

Core-shell Cu@Cu₂O nanoparticles on reduced graphene oxide (Cu@Cu₂O NPs-RGO) nanocomposite were prepared at room temperature by in situ reduction of graphene oxide (GO) and copper sulfate using *L*-ascorbic acid as reducing agent then air oxidation surface of copper nanoparticle. The Cu@Cu₂O NPs-RGO nanocomposite are characterized by infrared spectroscopy, Raman spectroscopy, X-ray diffraction, X-ray photoelectron spectroscopy, transmission electron microscopy, and energy dispersive X-ray spectroscopy. The Cu@Cu₂O NPs-RGO nanocomposite used as an efficient and reusable heterogeneous catalyst for *N*-Arylation of *N*-heterocycles.



Research highlight

- Core-shell Cu@Cu₂O nanoparticles on reduced graphene oxide (Cu@Cu₂O NPs-RGO).
- Ligand free *N*-Arylation of *N*-heterocycles under aerobic condition
- *N*-Arylation of *N*-heterocycles in short reaction time.
- EDS, FT-IR, Raman, SEM, TEM, XRD, and XPS characterization of Cu@Cu₂O NPs-RGO